Ocean Dynamics (2020) 70:977–990
https://doi.org/10.1007/s10236-020-01370-8

Modeling multiple wave systems in the eastern equatorial Pacific

Jesús Portilla-Yandún[1,2] · Andrés Salazar[3] · Jeison Sosa[4] · Sadid Latandret[5] · Luigi Cavaleri[6]

Received: 12 April 2019 / Accepted: 1 April 2020 / Published online: 27 May 2020

Abstract
While moderate wind and wave conditions prevail in the eastern equatorial Pacific, modeling waves in this area remains challenging due to the presence of multiple wave systems converging from different parts of the ocean. This area is covered by swells originated far away including the storm belts of both hemispheres, coexisting with local generation due to the regular action of both the southern trade winds and the wind jets from Central America. In this context, our ability to predict waves in the area depends on the overall quality (i.e., at Pacific scale) of the meteorological input, and also on the skills of the wave model itself. Clearly any error at the remote generation areas translates into larger errors the further waves go, especially if attention is focused on coastal areas. A relevant aspect is that the traditional integral parameters do not offer the possibility to properly assess the errors associated with the different parts of the spectrum (e.g., wind sea and swell). To gain insight in this direction, we make use of partitioning techniques, which enables us to neatly cross-assign and evaluate three spectral components. Not surprisingly, the performance for the swell part is lower than that of the corresponding wind sea. This is further explored with a couple of tests modifying both the wind input and the wave model physics. We find that although at first sight the initial scheme (i.e., ST4) seems to provide the better estimate, the spectral analysis reveals a substantial underestimation of wind sea, compensated with a substantial overestimation of swell. This suggests a problem with too high winds and wave generation in the storm belts together with a likely lack of dissipation or dispersion of swell. In turn, local waves are generally underestimated due to a corresponding underestimation of the local winds. This insight emphasizes the need and advantages of evaluation methods able to look at the different sectors of the wave spectrum.

Keywords Wave model evaluation · Partitioning · Wind waves · Swell · Eastern equatorial Pacific · Ecuador · Colombia

This article is part of the Topical Collection on the *International Conference of Marine Science ICMS2018, the 3rd Latin American Symposium on Water Waves (LatWaves 2018), Medellin, Colombia, 19-23 November 2018 and the XVIII National Seminar on Marine Sciences and Technologies (SENALMAR), Barranquilla, Colombia 22-25 October 2019*

Responsible Editor: Andrés Osorio

✉ Jesús Portilla-Yandún
jportilla@ymail.com

[1] Research Center of Mathematical Modelling (MODEMAT), Escuela Politécnica Nacional, Quito, Ecuador

[2] Department of Mechanical Engineering, Escuela Politécnica Nacional, Quito, Ecuador

[3] Department of Mechanical Engineering, Tokyo Institute of Technology, Tokyo, Japan

[4] School of Geographical Sciences, University of Bristol, Bristol, UK

[5] Dirección General Marítima de Colombia (DIMAR), Cartagena, Colombia

[6] Institute of Marine Sciences, ISMAR-CNR, Venice, Italy

1 Introduction

The focus of this work is in modeling waves in the eastern equatorial Pacific (henceforth EEP). This encompasses, by and large, the coasts of Colombia and Ecuador, as more detailed in Sect. 2 (see also Fig. 1a). From the practical point of view, the several coastal applications in the study area (e.g., harbor operations, coastal engineering, beach erosion, environmental studies) require in general wave conditions with high local resolution (because of local winds and especially complicated coastline and bathymetry) while depending on very large scale model results because the area is exposed to long swells, coming from the storm belts. These characteristics impose several challenges for wave modeling, being the first one related to the scale of the modeling domain, which necessarily has to cover the entire Pacific Ocean. Associated directly with this domain is the large range of wind speeds at work, including the highest on earth present in the storm belts, contrasting with the mild conditions typical at the equator.

At the same time, the wave model is also operating outside its comfort zone, of local active generation with predominant

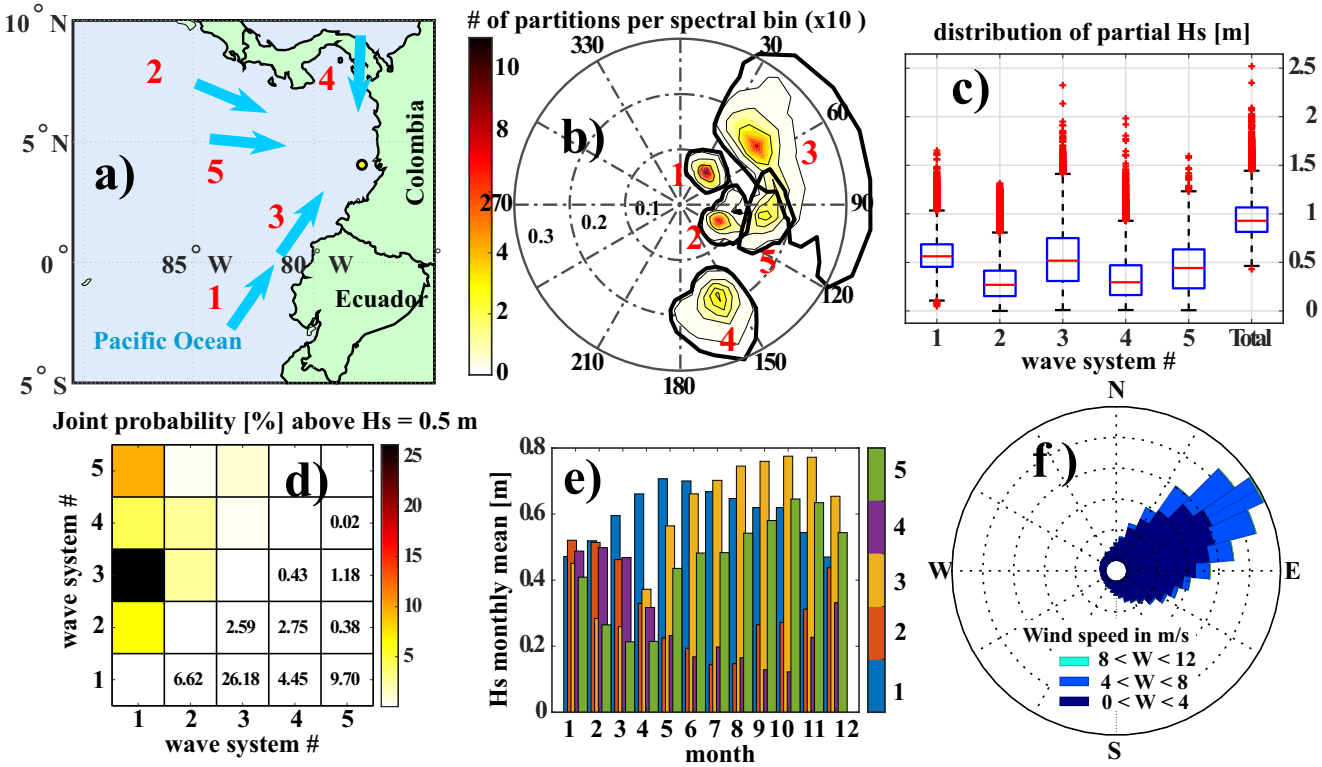

Fig. 1 Spectral wave characteristics in the EEP **a** regional map, **b** local wave systems (flow directions), **c** wave height statistics of the individual wave systems in **b**, **d** joint probability between pairs of wave systems, **e** monthly averaged wave heights, **f** wind rose in the area. Results from the GLOSWAC archive (reference point 4.0° N, 78° W)

unimodal spectral waves. Under such conditions, international weather centers report high-quality results from their operational wave models, see in this respect the statistics of NCEP (NCEP, 2019) and those of the European Centre for Medium-Range Weather Forecasts (Reading, U.K., ECMWF, 2018). However, processes like the far propagating energy or wave generation under mild wind conditions have till recently received comparably less attention (e.g., Ardhuin et al., 2019).

The modeling setup followed here is compatible with that presently used by the NOAA National Center for Environmental Prediction (NCEP, Maryland, USA), with a single general system covering the whole area of interest, plus a series of local nested grids, with progressively higher resolutions (Chawla and Tolman, 2008). The model is run on a central computer, using a single modeling software (i.e., the wave model WAVEWATCH III, Tolman et al., 2013). This setup is described in Sect. 3, where we also assess the quality of the wind input data and the related effects on the local wave model results.

It is observed that evaluating the model performance by total integral mean parameters (e.g., H_{m0}, T_m, θ_m) in complex spectral conditions is insufficient and sometimes misleading. Therefore, insight into the spectral structure is gained by using spectral partitioning approaches. This allows quantifying independently the errors related to the different parts of the spectrum, hence associated to different physical processes at work (e.g., generation and propagation). This analysis suggests the two experiments described in Sect. 4, acting respectively on the wind input and on the wave model.

Being representative of a common situation, we use the EEP for discussing the more general problem of local wave modeling in highly exposed areas, characterized by multimodal spectral wave conditions. It is from this perspective that the problem is going to be addressed, showing the practical difficulties in the study area and the accuracy we can expect, associated to both the wind input data and the possible shortcomings of present wave models. We provide a keen discussion on the derived results and the associated implications in Sect. 5, where we also summarize our main conclusions.

2 Preliminary assessment of the regional wave conditions

The area of interest is the west equatorial coast of South America, spanning the Pacific Ocean facing the coasts of Colombia and Ecuador, including the Galapagos Islands (see Figs. 1a and 2). For a preliminary assessment of the local wave conditions, we have made use of the GLOSWAC atlas (GLObal Spectral WAve Climate), which is an extensive

spectral characterization of the oceans based on long-term results of the ERA-I (nterim) reanalysis by the ECMWF (i.e., 37 years from 1979 to 2015). This provides a general overview of the wave climate in preparation of the wave modeling framework described in Sect. 3.

Figure 1 shows a set of typical indicators available from GLOSWAC, presented for a generic point representative of the whole area (4.0° N, 78° W). This point has been selected to be as close to the coast as the resolution of ERA-I allows it (i.e., 110 km). Figure 1 a displays a regional map, showing also the five main wave systems found in the area; these have been indicated with arrows to facilitate interpretation. These wave systems are derived from the information of Fig. 1b, which shows the long-term density distribution of partitions of all the ERA-I spectra. Note that this distribution is derived in the same (f, θ) domain as the original data, but is not a spectrum as such, being its measuring units: number of partitions per spectral bin (see Portilla-Yandún 2018 for a full description of this approach). Using this indicator, the long-term wave systems are defined from the clusters naturally emerging from this distribution. In turn, these can be associated to different meteorological origins (see also Table 1). In addition, given the specific and well-defined characteristics in the spectral domain (e.g., wave period and direction), it is possible to extract (from each cluster) many of their corresponding attributes (e.g., energy). Therefore, for each one of these wave systems, we have the full history of its wave heights. The resulting statistics for H_{m0} are given in the form of box-whisker plots in Fig. 1c, where the red lines correspond to the median, the boxes' limits indicate the 25th and 75th percentiles, and the whiskers are placed at 1.5 the interquartile range (IQR), marking the width of the distribution. In this representation, the mean value is generally near the 75th percentile. The red crosses can be considered part of the tail of the distribution (i.e., extremes). Note how the highest mean heights are associated to systems 1 and 3, but the possible extremes, reflected also in the overall distribution, come also from 2, 4, and 5. Particularly, system 4 shows a high number of extremes outside the IQR, suggesting a longer tail of its distribution in comparison with the other systems. Note also that the total H_{m0} has values higher than each of the individual systems both on average and in the extremes. This suggests a simultaneous occurrence of wave systems, which can be quantified by the joint probability between pairs shown in Fig. 1d. In this graphical representation, the upper diagonal shows in color what the lower diagonal displays numerically. The persistence of system 1 results in high joint occurrences with all the others. See for instance that the pair 1–3 has a relatively high occurrence probability (26%), followed by the pair 1–5 (10%). For a seasonal overview, the monthly average H_{m0} is given in Fig. 1e, showing a marked variability of each of these systems. In addition, the local winds can be assessed from the wind rose given in Fig. 1f.

Due to their frequent use, the cardinal directions will be indicated henceforth as N(orth), W(est), S(outh), and E(ast). Fully exposed to S, hence to swells from the Antarctic storm

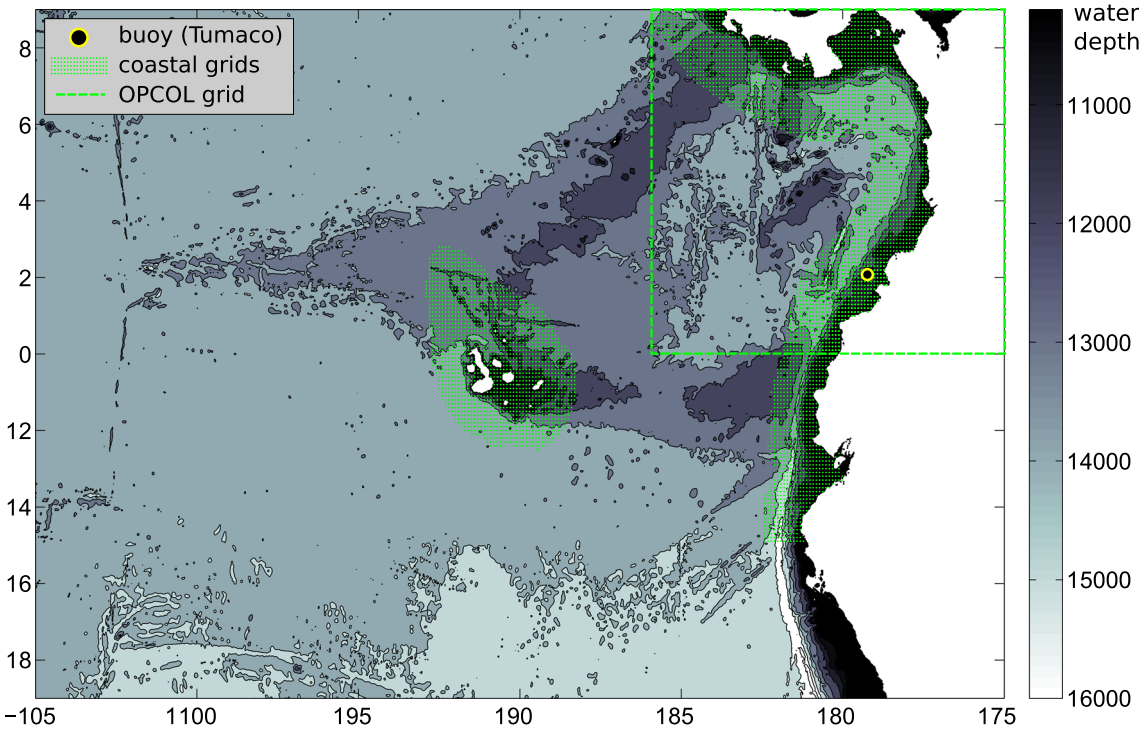

Fig. 2 Area of interest (latitude–longitude coordinates and bathymetry) for regional modeling (OPACE grid). The dashed green line indicates the OPCOL grid, the green dots indicate the coastal grids, yellow circle identifies the Tumaco buoy position (78° 52′ 55.11″ W 1° 54′ 14.19″ N)

Table 1 Incoming direction and genesis of the five wave systems identified in Fig. 1a

Number	Incoming direction	Genesis
1	South-West	Antarctic storm belt
2	West-North-West	Northern hemisphere storm belt
3	South-West	Trade winds
4	North	Panama jet
5	West	Westerlies

belt, wave system 1 makes on average the dominant condition, being the most persistent along the year, albeit with intermediate magnitudes (see Fig. 1e). Waves generated in the northern storm belt also reach the exposed coasts (system 2), although the area is partially shielded to N by Central and North America. There are also locally generated waves from S-W associated to the trade winds (system 3), which correspond to the dominant wind condition in the area (see also Fig. 1f). These are particularly strong during the austral spring months (Sep-Oct-Nov, see Fig. 1e). Note that although the primary direction of the trade winds in the south Pacific is from S-E, in their northward propagation along the South American coast (system 3 in Fig. 1a), they fade and fan out, getting gradually S directions around the Galapagos Islands and the S-W direction typical of the EEP. In addition, following the pressure difference between the Caribbean Sea and the EEP, rather energetic winds blow from N via the Panama strait (system 4, see e.g., Chelton et al., 2000). Finally, the moderate westerlies of the intertropical convergence zone (ITCZ) give origin to waves with similar characteristics (system 5). While Fig. 1 provides a climate overview derived from ERA-I, a more detailed description of the local wave conditions can be found in Portilla et al. (2015). Our purpose in the present paper concerns the forecasting of waves and therefore requires a more specific comparison between buoy data and model results. This is the subject of the next section.

3 Modeling waves in the eastern equatorial Pacific

3.1 Model set-up

Although most applications of interest take place in the coastal zone, given the just-described far-generated wave systems, wave modeling for the study area needs to cover the whole Pacific Ocean. Alternatively, one can use input boundary information from a regional grid (e.g. NCEP or ECMWF fields). However, on one hand, we meant to act as generally as possible, on the other hand, our long term purpose is the development of a local high resolution forecast system based on real-time available information (see https://modemat.epn.edu.ec/_nereo). For various reasons, this makes the choice of the whole Pacific Ocean more suitable, using the available wind forecasts from NCEP (see e.g., https://nomads.ncep.noaa.gov/) (note that at present the ECMWF forecast is not publicly available). Following this general line of action, a global 1° resolution grid has been set up, with two nested regional grids at 1/4° and 1/6° resolution and three coastal grids at 1/30° resolution. Figure 2 shows the regional nested area, indicating the coastal grids with high resolution. The overall grid characteristics are given in Table 2.

Verification data is available from buoys off the coast of Colombia (see Portilla et al. 2015 for specific details). These are Triaxys spherical buoys (1.10 m in diameter) based on accelerometers (see Shih, 2003; Skey and Miles, 1999). The 2D spectrum is derived using the maximum entropy method, MEM (see Nwogu, 1989), with a spectral resolution of 129 frequencies, from 0.0 to 0.64 Hz at regular intervals of 0.005 Hz, and 120 directions, from 0° to 360°, also at regular intervals of 3°. Particularly, the buoy at Tumaco contains good quality data for a continuous period of about 4 years (with only a few interruptions). The buoy location is indicated in Fig. 2 (yellow circle). The data are available at 1-h interval, with 2D spectra and all the derived parameters. The buoy was moored on 150 m of depth, still on the continental shelf extending till 50 km off the coast. The buoy was at its position from February 2009 till April 2013 (see Portilla et al. 2013 for details).

Bathymetry data were obtained from the Smith and Sandwell (1997) database at 2′ resolution. The model spectral domain is discretized in 25 frequencies ranging from 0.0412 to 0.4056 Hz with 1.1 geometric progression and 24 directions regularly distributed (at 15° step) starting from 7.5°. The WAVEWATCH III model has been used (Tolman et al., 2013; Tolman, 2014) in its 4.18 version using the so-called ST4 physics for the source terms (Ardhuin et al., 2010). In this parameterization, the wind input term (S_{in}) is similar to that from Janssen (1991), with a significant reduction at high frequencies to account for the unrealistic large drag coefficients at high wind speeds. The main characteristic of this formulation lies in the energy dissipation term (S_{dis}), which accounts for different effects including wave breaking and swell dissipation. Wave breaking is composed of a saturation-based term and a cumulative term to account for the breaking of short waves due to the breaking of long waves. In turn, swell dissipation includes a viscous and a turbulent components (see e.g., Ardhuin et al., 2010; Tolman, 2014 for details). Similar to other third generation parameterizations, ST4 also uses the discrete interactions approximation (DIA) from Hasselmann and Hasselmann (1985).

Wind field data and ice coverage in the polar areas correspond to forecast products from the NCEP Global Forecasting System (GFS, see Kalnay et al., 1990, or the NCEP online

Table 2 Characteristics of the overall and nested grids used for modeling the Pacific Ocean

	GLOBAL	OPACE	OPCOL	Coast 1 (OPACE)	Coast 2 (OPCOL)	Coast 3 (Galapagos)
Resolution deg (km)						
Latitude	1 (~ 111)	1/4 (~ 28)	1/6 (~ 18)	1/30 (~ 3.7)	1/30 (~ 3.7)	1/30 (~ 3.7)
Longitude	1 (~ 111)	1/4 (~ 28)	1/6 (~ 18)	1/30 (~ 3.7)	1/30 (~ 3.7)	1/30 (~ 3.7)
Coordinates						
Most northern lat. (deg)	78°	10°	0°	2.5°	0°	3°
Most southern lat. (deg)	− 78°	− 10°	10°	− 5°	10°	− 3°
Most eastern lon. (deg)	180°	− 75°	− 73°	− 78.5°	− 77.2°	− 88°
Most western lon. (deg)	− 180°	− 105°	− 86°	− 82.5°	− 86°	− 93°
Grid size	157 × 360	81 × 121	61 × 79	226 × 121	301 × 391	181 × 151

documentation at https://www.emc.ncep.noaa.gov/index.php?branch=GFS). Surface forecast wind fields are available on a regular 0.5° resolution grid at 3-h interval. The whole 4-year period for which buoy data is available has been considered for verification simulations. A discussion on the implications of a nonuniform quality of the wind data in this period is given in Sect. 5.

The specification of boundary conditions is greatly simplified using the multigrid capabilities of WAVEWATCH III, with the global and the successive nested grids exchanging information in two ways. As for initial conditions, it takes swells about 15 days to cross the oceans; therefore a warm-up period of about a month is generally sufficient for initialization. From there on, successive runs use the previous final state as initial condition.

3.2 Overall quality assessment of the wind input

For the purpose of assessing the quality of the input wind fields, we have used independent (i.e., not assimilated) scatterometer data from the Oceansat-2 mission (OSCAT). These are gridded data of wind vector cells (WVC) over the satellite swath, available at spatial resolutions of 50 and 25 km (see e.g., EUMESAT-OSISAF, 2018, and Martin, 2014 for specific details). Aiming at a general pattern, we use the OSCAT resolution of 50 km consistent with the GFS resolution. The time period is 1 year starting from the OSCAT onset date (i.e., October 2012) and partly overlapping the wave verification period. For data colocation, we use the satellite observations available between two model time steps (i.e., 3 h) and within each GFS grid, such that the average separation is lower than 1.5 h and 25 km. This results in an almost one to one match. Previous validations have reported average wind errors lower than 2 ms^{-1} and around 20° in direction (see Chakraborty et al. 2013; or online at http://projects.knmi.nl/scatterometer/). The usual scatter diagram of the overall GFS ocean comparison (see Fig. 3) suggests rather good agreement. Summarized into its essential statistical parameters (see the Appendix for definitions), we find a 0.91 R^2 fit (model vs. measurements), low bias (−0.04 ms^{-1}), and RMSE error (1.47 ms^{-1}) but a relatively large scatter index (SI = 0.18). This last figure suggests either a temporal or spatial variability in the fit. We explore this aspect observing the geographical distribution of the above parameters. Figure 3 reports the distribution of the RMSE, bias, and SI throughout the basin, summarized at a coarser level (5°), capable to convey the essential information at meso-scale, while keeping statistical efficiency. The most relevant information is the excess of energy in the storm belts (latitudes further than 40° from the equator), with large RMSE (around 2 ms^{-1}) and a positive bias around 1 ms^{-1}. There are also, as expected, large deviations (with strong negative bias) around areas with complex land-ocean configurations. A region of concern is the EEP region near Panama, involving the generation area of the local systems 3, 4, and 5 (see Table 1). Note also that the area of interest lies in the ITCZ where complex atmospheric convection processes play a dominant role (see e.g., Wallace and Hobbs, 2006) strongly complicating the local wind pattern. On the whole, there is a general tendency to overestimate the large wind speeds and to underestimate the low ones. On this basis, we move to the analysis of the wave model results.

3.3 Wave modeling results

The traditional intercomparison between model and buoy data is presented in Fig. 4: Fig. 4a for the significant wave height H_{m0} and Fig. 4b for the mean wave period $T_{m-1,0}$. By and large, the H_{m0} performance appears rather positive, with a best-fit slope slightly larger than unity. We have 10-cm positive bias, but (rather indicative) the scatter index is large (SI = 0.25), and the R^2 is low (0.57). Indeed, that the situation is not that simple is suggested by the $T_{m-1,0}$ scatter plot. It is obvious that on average, the model wave period is substantially overestimated, a big bunch of model results clustered between 7 and 8 s, versus the 5–6 s of the buoy (2 s positive bias). In this case too, the scatter index is large (SI = 0.40), with

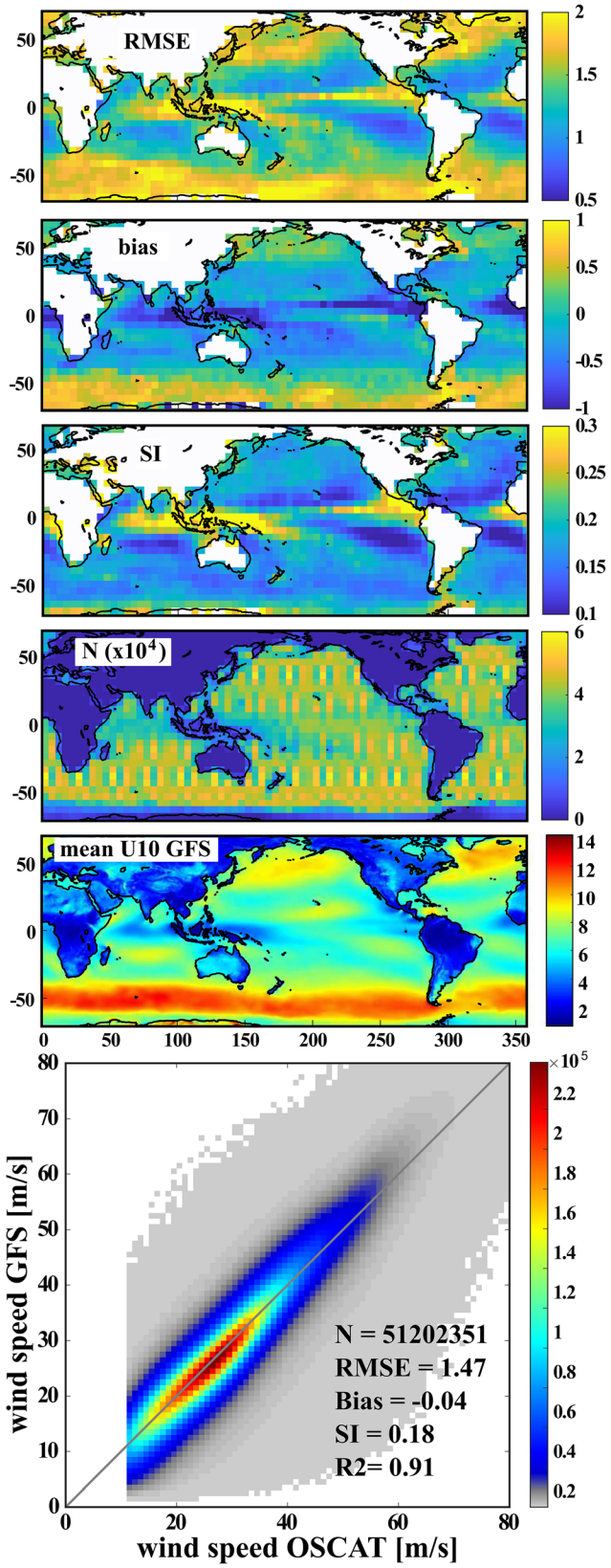

Fig. 3 Comparison between GFS forecast winds and scatterometer observations from OSCAT. Spatial distribution of RMSE (ms^{-1}), bias (ms^{-1}), scatter index (dimensionless), number of points, mean U10 from GFS (ms^{-1}), and overall scatter plot

relatively low R^2 (0.66). Note also that there is an apparent inconsistency in SI and R^2 between the two wave parameters. This is in part due to the fact that they penalize different characteristics in the comparison but also due to the limitation of integral parameters to portrait the general situation (see Sect. 4). However, the preliminary analysis of the local conditions strongly suggested that the presence of wave systems with different origins and characteristics requires a keener analysis of the results.

For this, we make use of spectral analysis techniques (see Portilla-Yandún et al. 2015). Similar to Fig. 1b, in Fig. 5, we report the resulting distribution of spectral partitions of our model results and the buoy data, obtained for the simulation period. Note again that these graphs do not report wave spectra but instead density distributions of partitions. Note also that although the magnitude of the variable (color scales) in each data source is significantly different, this is immaterial for the present purposes because the main objective here is to identify corresponding spectral clusters, for further coherent intercomparison (i.e., cross-assignment). On a parallel note, we owe to mention that these magnitude differences are not surprising, but they are inherent to the original data sets. Both the sources have different spectral and time resolutions, so they produce a different number of hits in each bin. Indeed, one advantage of the long-term spectral statistics technique is allowing the comparison of different data sources, respecting their native formats (see Portilla-Yandún et al. 2015).

In very good agreement with the long-term pattern obtained in the GLOSWAC distribution of Fig. 1, the model "spectral" signature of Fig. 5a shows well the five different wave systems previously identified. Although the situation is less clear in the buoy signature (Fig. 5b), the general configuration of both spectral distributions is very consistent. For a clear intercomparison, we search for corresponding conditions in both data sources that cross-assign well with each other. Indeed, the clearest match, given its separated spectral domain, is that of the Panama wind jet (system 4 in Fig. 1, and B in Fig. 5). The trade wind system (system 3 in 1, and C in 5) is also rather well defined in both the sources although with a larger data dispersion in the buoy. The most challenging comparison is that of the two swell systems (1 and 2 in Fig. 1) due to the poor definition in the buoy pattern (system A in Fig. 5). In Fig. 5b (green contour), we observe that these two systems are well defined in frequency (i.e., clearly separated from the trades and from the Panama systems) but not so well defined in direction, particularly between themselves as it is the case in the model signature (Fig. 5a). There are several possible reasons for that. At the buoy location, these waves may be actually affected by refraction, with both swells progressively aligning perpendicularly to the shore. However, since the continental slope of the area is very steep, the model, even at relatively high horizontal resolution and similar water depth conditions at the buoy location, is not able to capture these

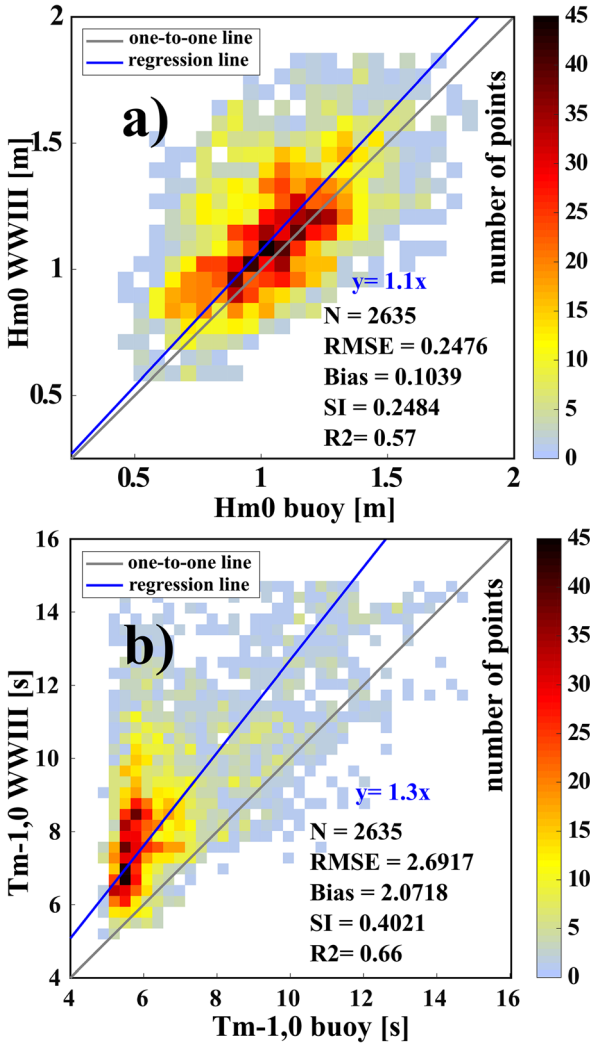

Fig. 4 Comparison between model and buoy measured significant wave height and mean period at the buoy location shown in Fig. 2. The time period is January 2010–December 2013

details due to limited vertical (bathymetry) resolution. On the other hand, processing numerical issues may also play a role because the buoy data has a much higher spectral resolution than the model, hence a larger data dispersion. In such cases, a much larger data set is needed for obtaining well-defined patterns from the buoy data (see Portilla-Yandún et al. 2015). Another possibility may be the limitation of the instrument to differentiate simultaneous swells in the same frequency range with different directions due to either the observing technique based on accelerometers or the MEM technique for deriving the 2D spectrum (see in this regard e.g., Donelan et al., 1985; Donelan et al., 2015 for a broader discussion on this subject). Furthermore, apart from these swell components, the westerly system (5 in Fig. 1) is also challenging but for a different reason. This system exists in both data sources, but its spectral domain connects and overlaps the N-W swells with the S-W trade winds (systems 2 and 3). Given all these conditions, in order to gain insight into the spectral structure without compromising precision (due to the lack of well-defined wave systems), the practical solution is to cluster the overlapping wave systems, hence considering fewer groups. For this purpose, we define the three systems A, B, and C, marked in Fig. 5. System A encompasses the three previously defined systems 1, 2, and 5. B corresponds to system 4 (Panama jet), and C to system 3 (trade winds). Given these definitions, we analyze the model performance for each of these components individually.

This comparison is presented in Fig. 6, panels a1, b1, and c1 for the corresponding wave heights and panels a2, b2, and c2 for the wave period. Concerning the wave heights, there is an obvious large overestimate of the swells (A), with most points clearly clustered in the upper diagonal (in a1), which results in 32-cm positive bias. The average model performance for systems B and C is better, showing a better

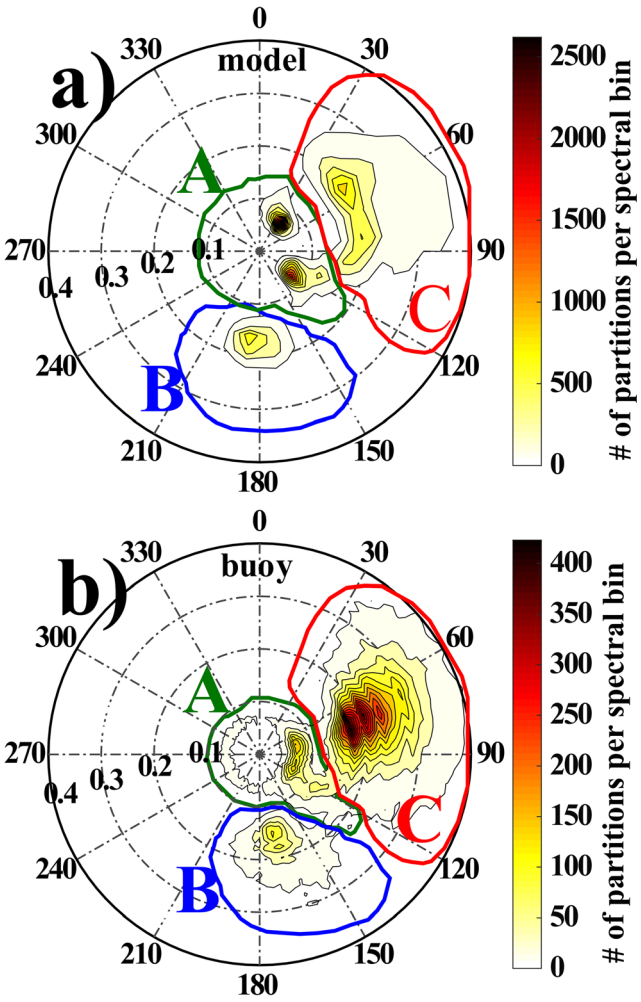

Fig. 5 Long-term distribution of the relevant wave systems acting at the buoy position in Fig. 2. **a** Model; **b** buoy data. A (swell), B (Panama), and C (trades) identify the three clusters used for evaluating the related performance

alignment of points over the diagonal (in b1 and c1), both are slightly underestimated (bias 0 and − 6 cm, respectively) but with a very large scatter (especially for B). Interesting enough, the performance is better for wave period in all the three cases, as compared with the total period of Fig. 4b. In particular, granted a limited amount of points (see the color scale), the distribution for A shows that the swell systems are well identified in time (otherwise, there would be large versus small values, and vice versa, in the comparison). So for swell, the problem appears to be mainly in the model excessive energy. For system B (the Panama jet), we find a slight excess in wave period, while the contrary, but with a large scatter, is the case for system C.

Whereas Fig. 6 provides a clear perspective of the performance of the single wave systems, this perspective is somehow biased by the different scales used in the various panels. So doing may be useful to highlight in the best way the single results, but it does not provide the overall view. In Fig. 7, we superimposed, for wave height and period, the data of the a, b, and c panels in Fig. 6. To better recognize the original three systems, we show with contours by and large the related distributions. The main message of these plots, including the overall best-fit lines, is that an apparently good fit does not necessarily imply a good performance of the model. Especially for wave height, the fit derives from compensating errors (see also Sect. 4 and Fig. 9), a message only partially conveyed by the large scatter index. Contrarily, the overall picture for the wave periods indicates a model performance significantly better than what was shown in Fig. 4. The comparison of the individual components is more consistent because in multimodal conditions, the wave period is very sensitive to the relative energy of the high and low frequency parts of the spectrum (wind sea and swell).

To convey better the information about the model performance for the three separate systems, we summarize in Table 3 the related RMSE, SI, and bias values individually reported in Figs. 4, 6, and 7. We see at once that the statistics of the integral parameters can be, and indeed is, misleading when different wave systems with different characteristics are present. In this respect, not as representative of the actual significant wave height but conveying a message on the actual performance of the model, it can be better to quantify the results provided by Fig. 7, which we report as "combined" in Table 3. It is easy to see that indeed these numbers provide a more objective view of the overall performance for the single wave systems. For instance, the 0.25-m RMSE for the integral parameters (H_{m0}) too optimistically represents the results of B and C (0.23 m and 0.26 m, respectively) while ignoring system A (0.4 m). The combined statistics (0.33 m) is more representative of the whole situation. Something similar occurs for the wave period, but contrarily in that case the integral parameters statistics offers a too pessimistic view.

Having framed the situation for the practical results, we need to identify the reasons for the model differences. The question is whether deficiencies come from the wind input (their later improvements with respect to the considered period will be discussed in the final Sect. 5) or from the wave model itself. Much of the attention of final users, and also modelers, is focused on the stormy areas and their local effects. Besides the obvious direct interest, this is also where it is

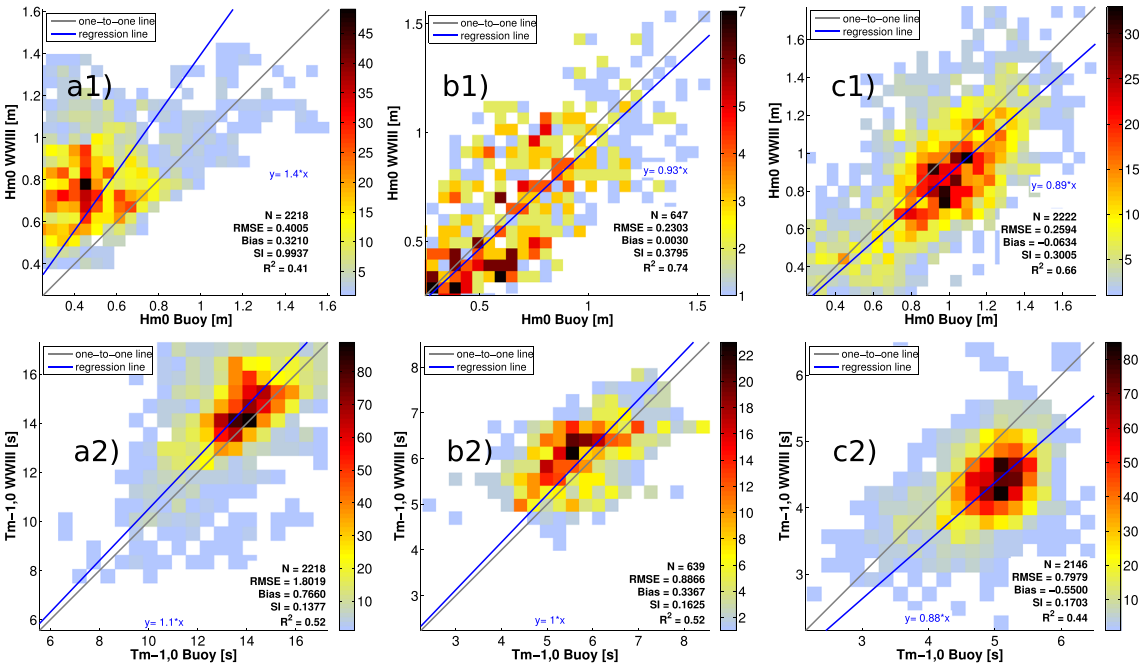

Fig. 6 Model vs. buoy comparison of the three wave systems identified in Fig. 5. Panels a, b, c for systems A (swell), B (Panama), C (trades); panels 1, 2 for wave height and mean period, respectively

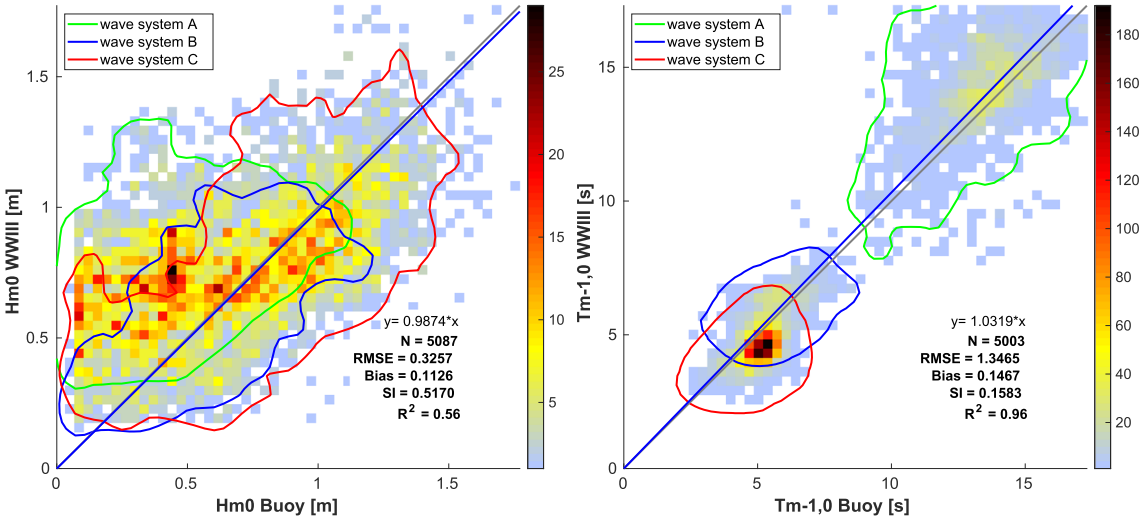

Fig. 7 Model vs. buoy comparison of the significant wave height and mean period at the location shown in Fig. 2. In each panel, the three contours indicate (approximately) the area covered by the A (swell), B (Panama), and C (trades) systems in Fig. 6. See Fig. 5 for their definition

easier to spot problems, both in wind and wave modeling, and to devise and test possible improvements, typically by calibrating the wind input. However, the present results show that waves generated in stormy areas evolve into swells that are less properly represented by the model in the remote areas. This is the condition in the equatorial zone, where we have a relatively low but persistent inflow of swell energy. Therefore, we have to work on long-term verification. We need to do this with general solutions, or at least, if not solutions (not within this paper), experiments capable to provide information on where to look for a solution. We have acted on both wind and waves. This is the subject of the next section.

4 Further numerical experiments

Given the overall modeling performance in the EEP, we have looked for possible solutions capable to hint where the basic problems lies. Our first attempt concerns the wind fields. We have seen (see Fig. 3) that the used wind speeds are in excess in the storm belts (hence the excess of swell) and possibly low in the local generation areas. On this basis, we apply an overall correction of the wind input derived from the global regression between OSCAT and GFS winds (given by $U' = 8/9\ U + 10/9$). This correction has the effect of reducing the high wind speeds and increase the low ones, whereas

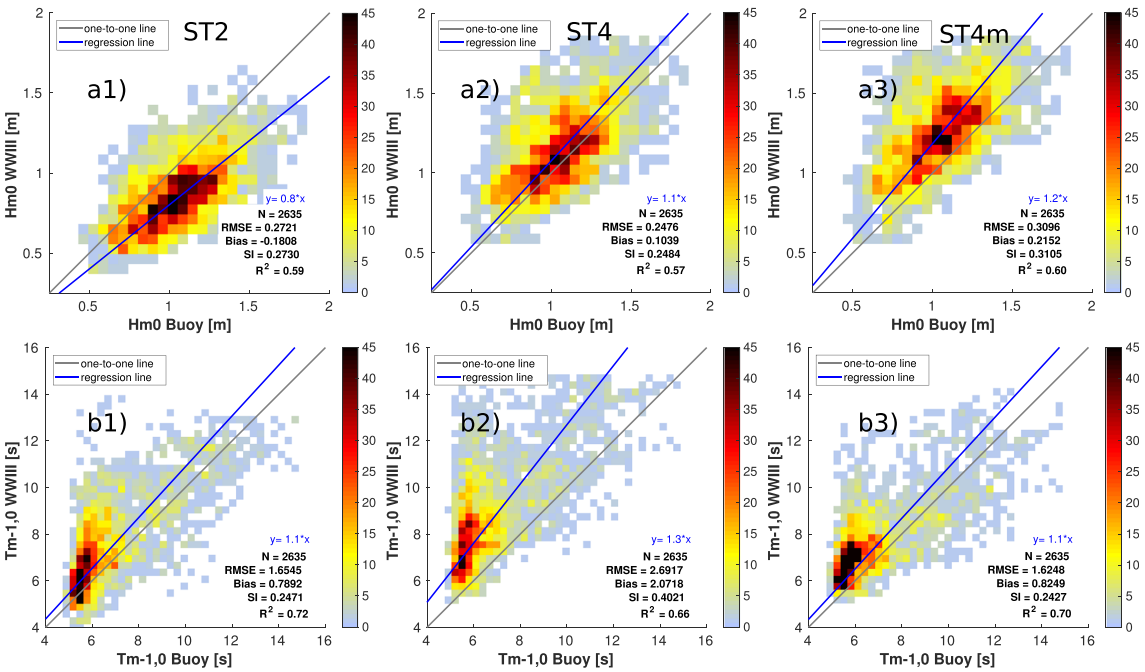

Fig. 8 Comparison between the H_{m0} and $T_{m-1,0}$ from the three different model approaches and the buoy measurements

Table 3 Performance (RMSE, SI, and bias) for significant wave height and mean period for the single systems A, B, C (see Fig. 5), their "combined" statistics, and the integral parameters (see the Appendix for definitions)

	H_{m0}			$T_{m-1,0}$		
	RMSE	SI	Bias	RMSE	SI	Bias
A (swell)	0.40	0.99	0.32	1.80	0.14	0.77
B (Panama)	0.23	0.38	0.00	0.89	0.16	0.34
C (trades)	0.26	0.30	− 0.06	0.80	0.17	− 0.55
Combined	0.33	0.52	0.11	1.35	0.16	0.15
Integral parameters	0.25	0.25	0.10	2.69	0.40	2.07

intermediate values are marginally affected. Note that several correction strategies are possible, including spatially localized parameters. However, although our main interest is focused on the EEP, we do not aim to force the system to get good results at the verification point, while probably neglecting the model performance at regional scale or in other locations of interest where presently there is no data available for verification. Using these adjusted wind fields, the model was run again keeping the original wave model setup (i.e., ST4). We further refer to this simulation as ST4m.

Turning to the wave model, the rational is the same, rather than tweaking with the many formulations available and their implied parameters, we have taken the step of using a different version of the WAVEWATCH III model, namely, the previous default package ST2 (Tolman and Chalikov, 1996). In comparison, ST4 was considered a substantial improvement, with different formulations of wind wave generation and dissipation, the latter also for long distance swell. However, the purpose of this approach is not to perform an intercomparison between the two formulations but rather to have a different wave modeling framework to assess the influence of the model while using the same winds. In this way, any difference between these two runs is only related to the wave model. We further refer to this simulation as ST2.

Following a similar analysis as in the previous sections, we compare at the buoy position the output of the three runs, namely, ST2, ST4, and ST4m. The related results for the overall H_{m0} and $T_{m-1,0}$, are presented in Fig. 8 (note that the central panels b1 and b2 for ST4 reproduce what is already shown in Fig. 4). The corresponding statistical parameters are compiled in Table 4 under the label "Integral parameters." In terms of H_{m0}, ST2 and ST4 seem comparable, except for the clear underestimate of ST2 (bias = − 0.18 m). In turn, ST4m does not seem to provide any appreciable improvement. However, the situation looks rather different from the $T_{m-1,0}$ perspective, for which both ST2 and ST4m provide systematically better results. Although the purpose here is not to judge which of the model runs was better than the others, this lack of performance consistency between H_{m0} and $T_{m-1,0}$ is problematic as it does not allow a proper assessment, more so because both the selected wave parameters are equally important.

In turn, the disaggregation of the wave spectrum into the subsystems (A, B, C) shows yet a different performance of the models for each wave system, allowing their individual quantification. The corresponding results are provided in Table 4, where also the "combined" results are included.

Looking at the individual components, we observe in general that ST4m is in all cases marginally different (better or worse). For system A, comparing ST4m with ST4, the reduction of the higher wind speeds, hence of the generated swells in the storm belts, is slightly beneficial (0.37 m vs. 0.40 m RMSE), but it is not yet sufficient to correct the overestimate of the swell at the buoy position (bias 0.27 vs. 0.32). Therefore, differently from the integral parameters point of view, we observe that the sensitivity of the results to the wind input is rather low. Note also that although we know system A is generated far away, its precise genesis location is difficult to assess as it is also the time of the storm. In general, we know that a substantial part of the energy comes from the southern

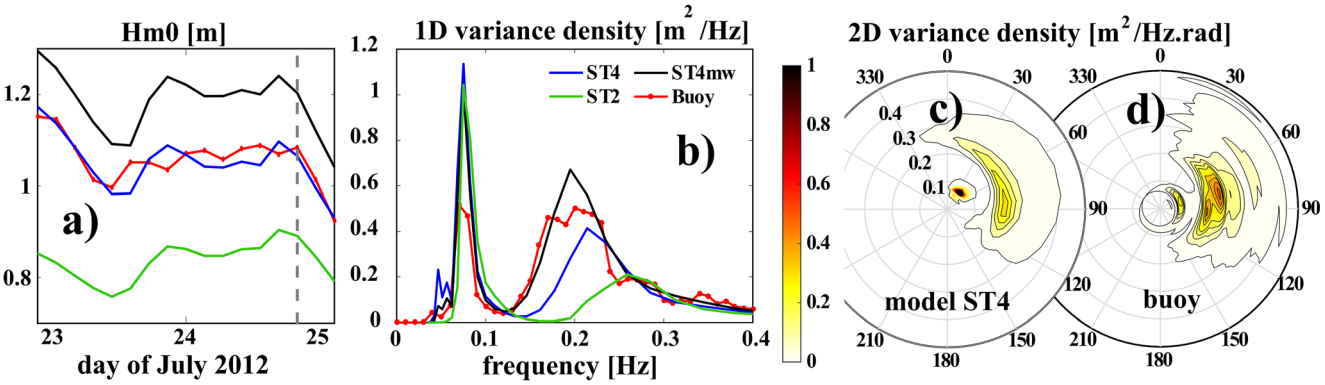

Fig. 9 **a** Comparison of recorded significant wave height at buoy position and the results of the three considered model approaches (ST2, ST4, ST4m). **b** Comparison of 1D spectra at the time marked in **a**. **c**, **d** ST4 and buoy 2D spectrum

Table 4 Performance (RMSE, bias, SI, and R^2, see the Appendix for definitions) for significant wave height and mean period for the three used model approaches vs. buoy data

		N	H_{m0}				$T_{m-1,0}$			
			RMSE	SI	Bias	R^2	RMSE	SI	Bias	R^2
A (swell)	ST2	2218	0.25	0.62	0.12	0.48	1.61	0.12	− 1.04	0.67
	ST4	2218	0.40	0.99	0.32	0.41	1.80	0.14	0.77	0.52
	ST4m	2218	0.37	0.93	0.27	0.34	1.82	0.14	0.20	0.49
B (Panama)	ST2	638	0.27	0.44	− 0.15	0.73	0.85	0.16	− 0.30	0.54
	ST4	647	0.23	0.38	0.00	0.74	0.89	0.16	0.34	0.52
	ST4m	649	0.24	0.39	0.05	0.74	0.92	0.17	0.45	0.55
C (trades)	ST2	2260	0.35	0.41	− 0.26	0.68	1.28	0.27	− 1.15	0.37
	ST4	2222	0.26	0.30	− 0.06	0.66	0.80	0.17	− 0.55	0.44
	ST4m	2310	0.28	0.34	0.13	0.71	0.60	0.13	− 0.20	0.54
Combined	ST2	5116	0.30	0.48	− 0.08	0.60	1.40	0.16	− 0.99	0.97
	ST4	5087	0.33	0.52	0.11	0.56	1.35	0.16	0.15	0.96
	ST4m	5177	0.32	0.52	0.18	0.70	1.31	0.16	0.06	0.96
Integral parameters	ST2	2635	0.27	0.27	− 0.18	0.59	1.66	0.25	0.79	0.72
	ST4	2635	0.25	0.25	0.10	0.57	2.69	0.40	2.07	0.66
	ST4m	2635	0.31	0.31	0.22	0.60	1.63	0.24	0.83	0.70

storm belt and also that the travel time is on average about 2 weeks. Based on these assumptions, the wind speeds in the active zone are estimated to be on the order of 15 ms^{-1}, which become 14.4 ms^{-1} in ST4m, so the wind modification is rather conservative (as it should be).

On the other hand, with respect to ST4, ST2 has a much reduced generation (bias 0.12 vs. 0.32), in a way partly correcting, but for a wrong reason (an intrinsic lower generation, see Fig. 9b), the swell excess in ST4. The low ST2 generation, although favorable for the swell system (A), is adverse for the local waves. We observe that the largest H_{m0} errors in this case correspond to system C (RMSE = 0.35 m), with the wave periods also significantly deteriorating (RMSE = 1.28 s).

To conclude this intercomparison, it is instructive to look at a specific record representative of the situations we have described. Figure 9 a shows the H_{m0} time series at the buoy location during few days of July 2012. We see the recorded significant wave heights and the corresponding results of the three considered approaches. At first glance, there is a perception of a good performance by ST4 (with hardly any difference from the recorded values). However, a closer inspection at the 1D spectra (Fig. 9b) tells another story. As in most of the cases, there is coexistence of wind sea and swell. ST4 underestimates the local wind sea while overestimating swell. Therefore, its apparent god fit derives from the mutual compensation of the two opposite errors. Note that none of the three approaches succeeds in capturing correctly the wind sea, the best result being the one of ST4m, following the slightly increased wind speeds (5.6 ms^{-1} with respect to 5.0 ms^{-1} of ST4). All the approaches overestimate at different levels the swell energy. Note that, as seen comparing Fig. 9 c and d and granted the large directional spreading of the measured swell, the general structure of the 2D spectrum is correct. This shows that the general structure of the wind fields is correct, both at large and local spatial scales. The problem is shared between a correct quantification of the wind in the different generation areas and the swell energy dissipation by the wave models.

A summary of the three different performances is: (a) as overall bias ST4 provides the best results, with ST2 under- and ST4m overestimating H_{m0} at the buoy location; (b) all the models overestimate the mean periods, a fact more evident for ST4; (c) the scatter is large, again particularly for $T_{m-1,0}$ of ST4. It seems therefore that none of the three approaches succeeds in providing high quality results in area of interest. This situation, the possible reasons why, if alternative solutions exist, or if the improvements in operational modeling can be the final solution, all these aspects are discussed in the final Sect. 5.

5 Discussion and summary

The results reported in the previous sections, for wave modeling in the eastern equatorial Pacific (EEP) point out to challenges due to the multimodal local conditions in this exposed area, where nesting a local model in large scale data covering the whole ocean does not suffice for providing satisfactory results. In wave modeling, much of the attention is on stormy areas and the related severe events. This is where wave models are usually tested; and one way or another, they succeed in

reproducing their main characteristics (e.g., Powell et al., 2010; Holthuijsen et al., 2012; Mori et al., 2014). In the equatorial Pacific area, the situation is different, wave conditions are dominated by the presence of long swells with relatively low energy, in coexistence with mild locally generated waves. Note that these are conditions where both the meteorological and wave models often do not perform at their best.

The analysis of the model performance in the equatorial zone, and more in general in areas where bimodal and multimodal wave conditions are regular, is difficult if focused only on overall H_{m0} or $T_{m-1,0}$. The example given in Fig. 9 is a typical case, not exclusive of the present study area. Although ST4 seems to provide the correct answer, a closer look at spectra tells another story: a substantial underestimation of wind sea is compensated with a substantial overestimation of swell. This situation emphasizes the need of evaluation methods able to look at the different sectors the wave spectrum. Knowing these problems, and also the results from the other two approaches (ST2 and ST4m), the overall message is clear: there is a problem with too high winds and wave generation in the storm belts together with a likely lack of dissipation or dispersion of swell during its long voyage toward the equatorial zone. In turn, local waves were underestimated due to a corresponding underestimation of the local winds.

Following the continuous developments of international centers (e.g., GFS, NCEP, and ECMWF), one finds that the forecast capability improves asymptotically in time, at a rate of about 1 day per decade (see, e.g. Cavaleri et al., 2018; ECMWF, 2018; NCEP, 2019). However, problems remain, especially in the equatorial zone (see e.g., Kerns and Chen, 2014), where the advection of long-distance swells is a key and critical point. The following stage of WAVEWATCH III, ST6, includes substantial improvements both in physics and numerics, especially in active wind conditions. See for instance the exhaustive overview given by Stopa et al. (2015), where they also point out to challenges in modeling swell. This is in part related to the difficulty in properly describing the energy directional spread even at the generation area. It is obvious that any small error in the source area will correspond to more drastic ones the further waves go. While ST6 was not yet available when this work was started, the picture provided by Stopa et al. (2015) strongly suggests that, at least for swell in the equatorial zone, ST6 may not be yet the final solution. If we then move closer to coast, possibly with complicated local bathymetry and orography, it is clear that the problem worsens. In addition, swell history may be affected by ocean currents. However, while large scale models can represent relatively well the large scale currents, it is extremely difficult to do so moving to the smaller scales, however still large enough to affect the swell propagation.

On the other hand, the different model performances for sectors of the spectrum associated to different generation zones indicate the complexity of the wind field structure. Whereas the ad hoc wind correction tested here hint to the possible modifications needed, a rigorous correction can only be achieved through comprehensive wind and wave data assimilation approaches. This may be at present the most effective mechanism to improve wave predictions in the study area. This should be favored in the near future by the increasing availability of good quality SAR spectra from different satellites.

We itemize our conclusions as follows:

1. Wave modeling has focused for a long while on the most relevant and strong events and implicitly on the physics of the generation zone. Only in more recent times and for practical purposes, attention has moved to swell, especially on the tropical and equatorial zone.
2. Apart from the local moderate wind conditions, modeling waves in the eastern equatorial Pacific deals primarily with long-distance swells arriving from different regions of the ocean, including both the South and North storm belts. Therefore, modeling errors in this zone include those corresponding to local generation, plus the ones related to the far generating zones, often amplified in the propagation process. Although the magnitudes of these two components are comparable, the quantification shows that swell errors are about twice as large as those of local waves.
3. Two experimental approaches were tested, using the WAVEWATCH III model. The first attempted a correction of the generating wind fields using the same model setup (ST4m), and the second used the original wind fields, with a different model setup (ST2). Although no substantial improvement or deterioration of the results was observed, these tests were useful in showing the response of the modeling system due the wind input and to the model physics.
4. In areas where wave conditions are characterized by multiple wave systems, overall integral wave parameters give a distorted picture of the real situation (H_{m0} tends to hide errors, while $T_{m-1,0}$ tends to exaggerate them). We show that spectral model evaluation based on partitioning methods provides a more objective view of the model performance, hence of the related physics. The detailed assessment for the different sectors of the spectrum allows to better identify and quantify the source of errors associated to different processes (e.g., local wind generation, propagation).

Acknowledgments Forecast GFS winds and polar ice concentrations were downloaded from the NOAA Operational Model Archive and Distribution System (NOMADS). OSCAT winds were downloaded from the OSI-SAF, KNMI archive. GLOSWAC information was obtained from its web site (https://modemat.epn.edu.ec/nereo/). ERA-I data and forecast statistics were obtained from the ECMWF web site. Buoy data

was provided by the Dirección General Marítima de Colombia (DIMAR). Global bathymetry was downloaded from the National Centers for Environmental Information. J. Portilla acknowledges funding from project EPN-PIJ-1503. We acknowledge the insight of the anonymous reviewers for helping improve the final quality of the manuscript.

Appendix. Statistical parameters

The statistical parameters for comparisons between model results and observations are root mean square error (RMSE), bias, scatter index (SI), and the coefficient of determination (R^2). The corresponding formulations as given by Van Vledder (1993) are:

$$RMSE = \left\{ \frac{1}{N} \sum_{i=1}^{N} (x_i - y_i)^2 \right\}^{1/2} \tag{1}$$

$$BIAS = \frac{1}{N} \sum_{i=1}^{N} (y_i - x_i) \tag{2}$$

$$SI = \frac{RMSE}{\left| \overline{x} \right|} \tag{3}$$

$$R_{x,y} = \frac{\sum_{i=1}^{N} \left(x_i - \overline{x} \right) \left(y_i - \overline{y} \right)}{\left\{ \sum_{i=1}^{N} \left(x_i - \overline{x} \right)^2 \right\}^{1/2} \left\{ \sum_{i=1}^{N} \left(y_i - \overline{y} \right)^2 \right\}^{1/2}} \tag{4}$$

where x is the measured and y the modeled variable.

References

Ardhuin F, Rogers E, Babanin AV, Filipot J, Magne R, Roland A, van der Westhuysen A, Queffeulou P, Lefevre J, Aouf L, Collard F (2010) Semiempirical dissipation source functions for ocean waves. Part I: definition, calibration, and validation. J Phys Oceanogr 40:1917–1941. https://doi.org/10.1175/2010JPO4324.1

Ardhuin F, Stopa JE, Chapron B, Collard F, Jensen RE, Johannessen J et al (2019) Observing sea states. Front Mar Sci 6:124. https://doi.org/10.3389/fmars.2019.00124

Cavaleri L, Abdalla S, Benetazzo A, Bertotti L, Bidlot J-R, Breivik Ø, Carniel S, Jensen RE, Portilla-Yandun J, Rogers WE, Roland A, Sanchez-Arcilla A, Smith JM, Staneva J, Toledo Y, van Vledder GP, van der Westhuysen AJ (2018) Wave modelling in coastal and inner seas. Prog Oceanogr V167:164–233. https://doi.org/10.1016/j.pocean.2018.03.010

Chakraborty A, Kumar R, Stoffelen A (2013) Validation of ocean surface winds from the OCEANSAT-2 scatterometer using triple collocation. Remote Sens Lett 4(1):84–93. https://doi.org/10.1080/2150704X.2012.693967

Chawla A, Tolman H (2008) Obstruction grids for spectral wave models, J. Ocean Model V22(I1–2):12–25. https://doi.org/10.1016/j.ocemod.2008.01.003

Chelton DB, Freilich M, Esbensen S (2000) Satellite observations of the wind jets off the Pacific coast of Central America, part II: regional relationships and dynamical considerations. Mon Weather Rev 128: 2019–2043. https://doi.org/10.1175/1520-0493(2000)128%3C1993:SOOTWJ%3E2.0.CO;2

Donelan MA, Hamilton J, Hui WH (1985) Directional spectra of wind-generated waves. Philos Trans R Soc Lond A 315:509–562

Donelan M, Babanin A, Sanina E, Chalikov D (2015) A comparison of methods for estimating directional spectra of surface waves. J Geophys Res Oceans 120:5040–5053. https://doi.org/10.1002/2015JC010808

ECMWF, 2018. https://www.ecmwf.int/en/newsletter/154/news/forecast-performance-2017 , Forecast performance 2017, Newsletter 154, (on-line). Last accessed 2019-09-02

EUMESAT-OSISAF, (2018). ScatSat-1 wind Product User Manual Version: 1.3. http://projects.knmi.nl/scatterometer/publications/pdf/osisaf_cdop2_ss3_pum_scatsat1_winds.pdf

Hasselmann S, Hasselmann K (1985) Computation and parameterizations of the nonlinear energy transfer in a gravity-wave spectrum. Part I: a new method for efficient computations of the exact nonlinear transfer. J Phys Oceanogr 15:1369–1377

Holthuijsen L, Powell M, Pietrzak J (2012) Wind and waves in extreme hurricanes. J Geophys Res 117:C09003. https://doi.org/10.1029/2012JC007983

Janssen PAEM (1991) Quasi-linear theory of wind wave generation applied to wave forecasting. J Phys Oceanogr 21:1631–1642

Kalnay E, Kanamitsu M, Baker W (1990) Global numerical weather prediction at the National Meteorological Center. Bull Amer Meteor Soc 71:1410–1428

Kerns B, Chen S (2014) ECMWF and GFS model forecast verification during DYNAMO: multiscale variability in MJO initiation over the equatorial Indian Ocean. J Geophys Res Atmos 119:3736–3755. https://doi.org/10.1002/2013JD020833

Martin S (2014) An introduction to ocean remote sensing. Cambridge University Press ISBN 9781107019386, 496 pp

Mori N, Kato M, Kim S, Mase H, Shibutani Y, Takemi T, Tsuboki K, Yasuda T (2014) Local amplification of storm surge by Super Typhoon Haiyan in Leyte Gulf. Geophys Res Lett 41:5106–5113. https://doi.org/10.1002/2014GL060689

NCEP, 2019. https://www.emc.ncep.noaa.gov/gmb/STATS_vsdb/. NCEP/EMC global model experimental forecast performance statistics (on-line). Last accessed 2019-09-02

Nwogu O (1989) Maximum entropy estimation of directional wave spectra from an array of wave probes. Appl Ocean Res 11:176–182. https://doi.org/10.1016/0141-1187(89)90016-3

Portilla J, Caicedo A, Padilla-Hernández R (2013) Observations of directional wave spectra in the Colombian Pacific. Rev Avances USFQ. https://doi.org/10.18272/aci.v5i2.137. https://www.usfq.edu.ec/publicaciones/avances/archivo_de_contenidos/Documents/volumen_5_numero_2/c5_5_2_2013.pdf

Portilla J, Caicedo-Laurido A, Padilla-Hernández R, Cavaleri L (2015) Spectral wave conditions in the Colombian Pacific. Ocean Model 92:149–168. https://doi.org/10.1016/j.ocemod.2015.06.005

Portilla-Yandún J, Cavaleri L, van Vledder GP (2015) Wave spectra partitioning and long term statistical distribution. Ocean Model 96: 148–160. https://doi.org/10.1016/j.ocemod.2015.06.008

Portilla-Yandún J (2018) The global signature of ocean wave spectra. Geophys Res Lett 45:267–276. https://doi.org/10.1002/2017GL076431

Powell, M., , S. Murillo, P. Dodge, E. Uhlhorn, J. Gamache, V. Cardone, A. Cox, S. Otero, N. Carrasco, B. Annane, R. Fleur, (2010). Reconstruction of hurricane Katrina's wind fields for storm surge and wave hindcasting, Ocean Eng, 37, 26–36, https://doi.org/10.1016/j.oceaneng.2009.08.014

Shih H., 2003. Triaxys directional wave buoy for nearshore wave measurements – test and evaluation plan, NOAA Technical Report NOS CO-OPS 38 Silver Spring https://repository.library.noaa.gov/view/noaa/14670

Skey, S., Miles, M., 1999. Advances in buoy technology for wind/wave data collection and analysis, OCEANS'99MTS/IEEE.RidingtheCrestintothe21stCentury 1,113–118.doi:https://doi.

org/10.1109/OCEANS.1999.799716, http://ieeexplore.ieee.org/xpl/freeabs_all.jsp?arnumber=799716&abstractAccess=no&userType=inst

Smith W, Sandwell D (1997) Global seafloor topography from satellite altimetry and ship depth soundings. Science 277:1956–1962. https://doi.org/10.1126/science.277.5334.1956

Stopa J, Ardhuin F, Babanin A, Zieger S (2015) Comparison and validation of physical wave parameterizations in spectral wave models. Ocean Model V103:2–17. https://doi.org/10.1016/j.ocemod.2015.09.003

Tolman H, Chalikov D (1996) Source terms in a third-generation wind-wave model. J Phys Oceanogr 26:2497–2518. https://doi.org/10.1175/1520-0485(1996)026%3C2497:STIATG%3E2.0.CO;2

Tolman H, Banner M, Kaihatu J (2013) The NOPP operational wave model improvement project. Ocean Model 70:2–10. https://doi.org/10.1016/j.ocemod.2012.11.011

Tolman H., (2014). User manual and system documentation of WAVEWATCH III, technical note, Environmental Modeling Center Marine Modeling and Analysis Branch MMAB Contribution No 316

Van Vledder GP (1993) Evaluation of model performance (methodology, examples, subroutines). Delft Hydraulics, Delft

Wallace J, Hobbs P (2006) Atmospheric science, second edition: an introductory survey (international geophysics), 2nd edn. Academic Press, p 504 ISBN: 978-0127329512